Impact of Atmospheric Aerosols on the Accuracy of IMERG Precipitation Estimates Over Northern China

Xiaoying Li, Sungmin O, Na Wang, Lichen Liu, and Yinzhou Huang

***Abstract*—Accurate satellite precipitation estimates are vital for understanding global and large-scale regional water cycles. Among the many factors influencing satellite precipitation data quality, the detection and accuracy of precipitation products at different atmospheric aerosol concentrations are not well studied. In this study, we investigated the impact of atmospheric aerosols on the accuracy of satellite precipitation products (IMERG) over North China by comparing performance metrics such as bias, normalized root mean squared error, probability of detection (POD), and false alarm ratio (FAR) under different atmospheric aerosol conditions. The results revealed that IMERG generally exhibits poorer detectability and quantification under pollution condition. Based on the error decomposition, the estimated errors in autumn and winter were dominated by false biases, which are mainly affected by atmospheric aerosols. At the sensor level, the FARs of both infrared (IR) and passive microwave sensors show escalating trends as pollutant concentrations increase. The POD of IR sensors is affected by pollution. Pollution has a significant impact on IR detection capability. Our findings suggest that atmospheric aerosols may impact the accuracy of IMERG precipitation estimates over Northern China and need to be taken into consideration in the IMERG retrieval process and data utilization.**

***Index Terms*—Atmospheric aerosols, detectability, IMERG, North China (NC), precipitation estimates.**

I. Introduction

PRECIPITATION is a fundamental component of the global water cycle, crucial for understanding hydrological processes and climate change impacts on water resources [1], [2]. Therefore, reliable precipitation data are vital for agricultural and hydrological studies, water resource management, and climate-related applications [3].

In addition to ground-based gauge observations or radar remote sensing, which are two sources that are widely used for near real-time collection of precipitation information, satellite precipitation products (SPPs) have become an indispensable source of precipitation estimation at a large-scale across the globe [4], [5]. As a new generation of satellite-based retrieval products, the IMERG product provides quasi-global precipitation data at a high level of spatio-temporal resolution [6], [7]. In particular, GPM IMERG is better suited for capturing solid precipitation and light precipitation [8], [9], [10], [11]. Since its first release in 2014, the IMERG dataset has been utilized in various hydrological applications [12], [13], [14], [15]. To assess the data quality and guide further improvements, GPM IMERG has been extensively evaluated through comparison with ground-based observational data. Many studies have reported its error characteristics and identified factors that can affect retrieval accuracy [16], [17], [18], [19].

Various studies have explored the performance of IMERG under different climatic factors, topographic conditions, and precipitation phases [20], [21]. However, the detection and accuracy of IMERG precipitation products at different atmospheric aerosol concentrations are poorly understood. Aerosols can affect precipitation processes in complex ways, influencing cloud properties and the formation of precipitation, and, thereby, they can alter the precipitation efficiency of clouds [22], [23], [24]. Increased complexities in cloud-water systems under the influence of aerosols bring more uncertainties to satellite precipitation detection. Notably, no study has yet examined the impacts of varying aerosol levels on IMERG precipitation detection accuracy. To fill this research gap, this study focuses on the detection accuracy of IMERG products under different aerosol concentrations, in order to comprehensively assess the impact of aerosols on satellite precipitation detection and improve the robustness of precipitation estimation algorithms.

The purpose of this study is: 1) to investigate the accuracy of the IMERG data under different atmospheric aerosol concentrations; and 2) to reveal error sources and quantify the error magnitudes of IMERG under pollution conditions.

This study is structured as follows. The study area and data sources are introduced in Section II. Section III presents the statistical metrics used in the study. Section IV details the results and discussion. Finally, Section V summarizes the main conclusions.

II. Study Area, Used Data

A. Study Area

North China (NC), encompassing the metropolitan areas of Beijing and Tianjin and part of the provinces with rapid

Manuscript received 26 August 2023; revised 20 November 2023; accepted 12 January 2024. Date of publication 19 January 2024; date of current version 2 February 2024. This work was supported by the National Natural Science Foundation of China under Grant 42201016 and Grant 41971195. The work of S. O was supported by the Basic Science Research Program through the National Research Foundation of Korea (RS-2023-00248706). *(Corresponding authors: Xiaoying Li; Lichen Liu.)*

Xiaoying Li, Lichen Liu, and Yinzhou Huang are with the College of Earth and Environmental Sciences, Lanzhou University, Lanzhou 730000, China (e-mail: lixiaoying@lzu.edu.cn; liulch@lzu.edu.cn; yzhhuang@lzu.edu.cn).

Sungmin O is with the Department of Climate and Energy Systems Engineering, Ewha Womans University Seoul 03760, South Korea (e-mail: sungmin.o@ewha.ac.kr).

Na Wang is with the Shaanxi Climate Center, Xi'an 710016, China (e-mail: wangna_na@163.com).

Digital Object Identifier 10.1109/JSTARS.2024.3356256

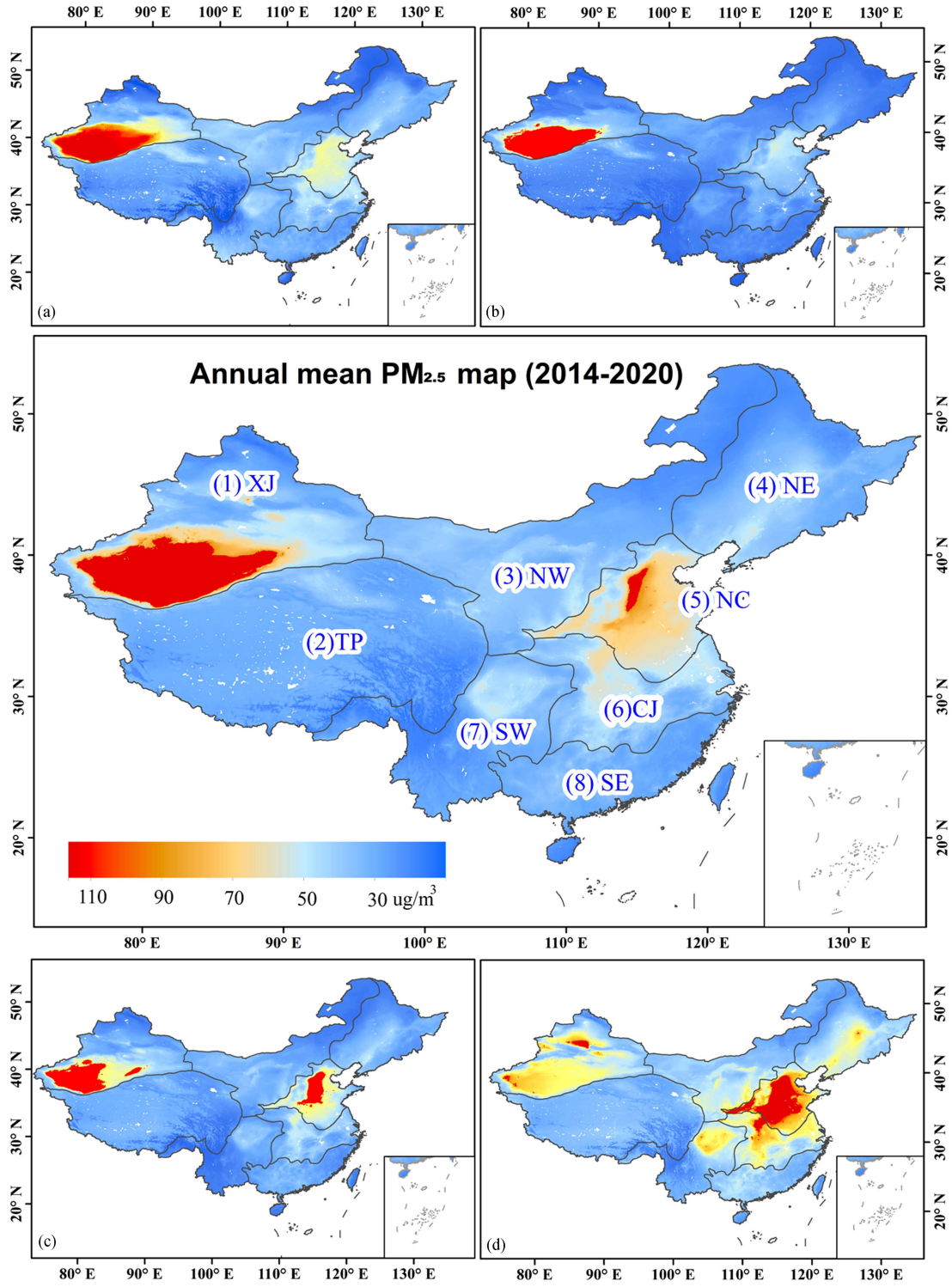

Fig. 1. Annual mean 1 km-resolution $PM_{2.5}$ map and seasonal mean 1 km-resolution PM2.5 maps (a) Spring, (b)Summer, (c) Autumn and (d) Winter averaged over the period 2014–2020. NC shows a remarkably higher aerosol concentration than other subregions. The eight regions include the Xinjiang (XJ), North China (NC), Southwestern China (SW), Southeast China (SE), Tibetan Plateau (TP), Northeast China (NE), Northwestern China (NW), and Changjiang (Yangtze) River (CJ).

industrialization and urbanization [25], consists of groups of large, nearly contiguous cities [26]. Due to its dense population and anthropogenic emission sources (e.g., from industrial activities, motor vehicle exhaust, and biomass burning), the NC region (Fig. 1) frequently suffers from serious aerosol pollution [27], [28].

The NC area is therefore suitable for exploring the accuracy of SPPs under the impact of atmospheric aerosols. Fine particulate

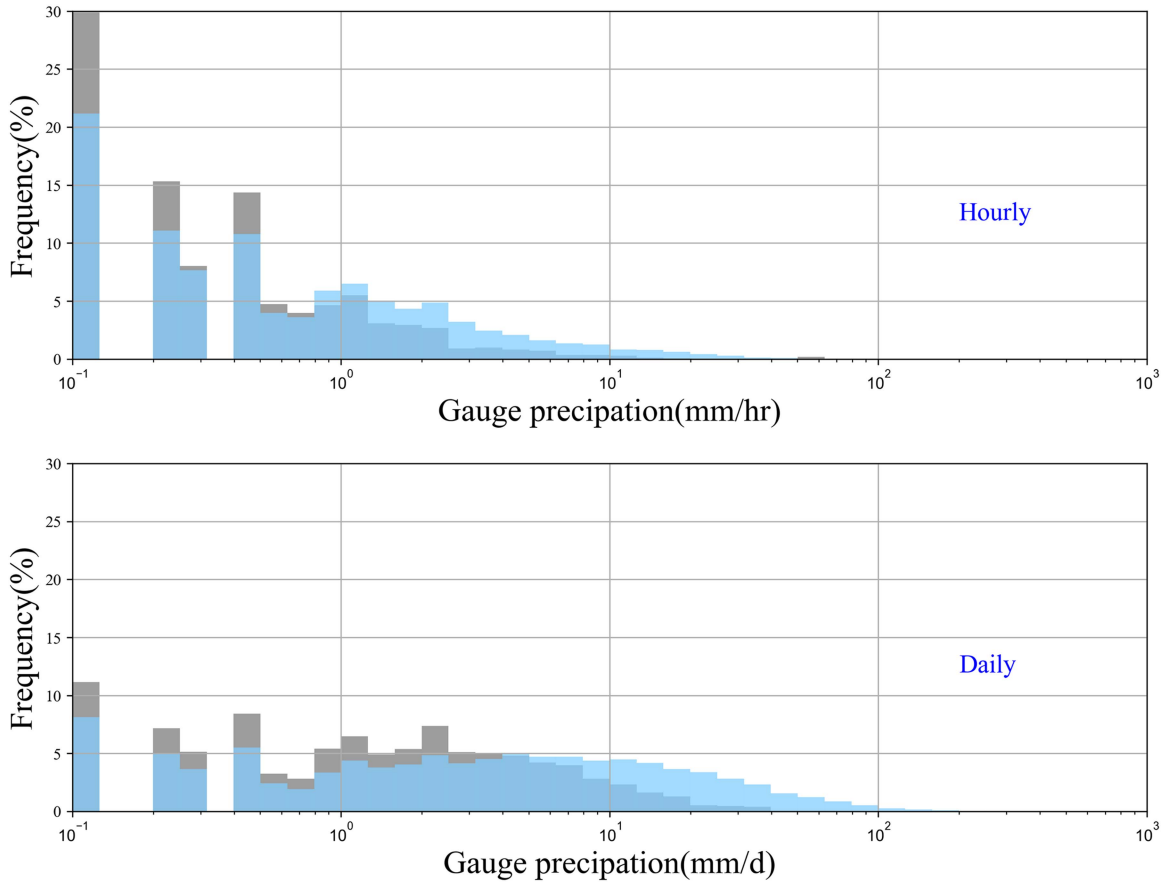

Fig. 2. Frequency of hourly and daily precipitation under clean (blue) and polluted (gray) conditions derived from combined winter and autumn data.

matter ($PM_{2.5}$) is a precursor to air pollution [29]. Particularly high $PM_{2.5}$ concentrations were observed in winter (December, January, and February), as shown in Fig. 1(d) and autumn (September, October, and November), as shown in Fig. 1(c). The concentrations of $PM_{2.5}$ in winter are evidently higher than in other seasons (Fig. 1) due to stronger emissions related to heating for residential areas and stable atmospheric stratification [30], [31]. In this study, autumn and winter were chosen as the main study periods.

B. Precipitation Datasets

1) Precipitation Gauge Dataset: Daily and hourly precipitation data collected from gauges over the NC region for the period of January 1, 2014 through December 31, 2020 have been used as the reference data to assess the quality of IMERG in this study. The China Meteorological Administration (CMA) supplied quality management for the observation data. The resolution of the rain gauges was 0.1 mm/h.

Fig. 2 displays the frequency of daily and hourly precipitation recorded by gauge monitoring stations under clean and polluted conditions from both fall and winter seasons during the study period over NC. For hourly rain events in winter and autumn, the vast majority of precipitation events were less than 10 mm/h. Based on the precipitation characteristics shown in Fig. 2, the hourly precipitation events with less than 10 mm/h were selected for the hourly scale study.

The two main precipitation intensities for the daily scale study were drizzle (<1 mm/d) and light precipitation (<10 mm/d) in winter and autumn both on polluted and clean days, as they were the most common precipitation events.

2) Satellite Precipitation Dataset: IMERG V06B is high-resolution multi-SPPs which has a $0.1° \times 0.1°$ spatial resolution and a 30-min temporal in three runs: IMERG-early, IMERG-Late, and IMERG-Final [32]. The IMERG-Final precipitation products are generated using two types of input data.

The gauge-adjusted products (PrecipitationCal) incorporate monthly precipitation data from the Global Precipitation Climatology Centre to adjust and improve the accuracy of satellite precipitation estimates.

The uncalibrated products (PrecipitationUnCal) are derived directly from different satellite precipitation estimation algorithms without gauge adjustment [33].

In this article, we chose the IMERG Final Run Version 06B PrecipitationUnCal products. And in order to better evaluate the impact of atmospheric aerosols on different data sources estimates, IMERG pixels were categorized into three groups based on their KF weights value. 1) Pixels with a KF-weight of 100% [infrared (IR)-only estimates]; 2) Pixels with a KF-weight of 0% [passive microwave (PMW)-only observations]; and

3) Pixels with a KF-weight between 0 and 100% (a mixture of PMW and IR). We set the precipitation detection threshold of IMERG estimates to be 0.1 mm/h to distinguish rain and no-rain events. The threshold represents the minimum rainfall rate that IMERG can detect, i.e., the resolution of IMERG precipitation estimates [34].

3) Air Monitoring Data: The daily atmospheric aerosols data with a 1-km resolution from 2014 to 2020 were obtained from the China High Air Pollutants dataset, which has been verified to be highly accurate and has been used in relevant studies [35], [36]. To investigate the impact of daily atmospheric aerosol concentrations on the accuracy of daily IMERG precipitation estimates, we categorized concentrations of daily $PM_{2.5}$ into two groups: 1) clean day, when daily $PM_{2.5}$ concentration was less than 75 $\mu g/m^3$; and 2) pollution day, when the daily $PM_{2.5}$ concentration was above 75 $\mu g/m^3$.

Hourly atmospheric aerosol data were collected from the air monitoring gauges established by the Ministry of Ecology and Environment of China. The air monitoring network now includes more than 1650 sites located in 278 cities and regions in China [37]. There are 473 air monitoring sites in NC. To reduce errors in the monitoring network dataset due to the lack of quality control before 2017, hourly ambient mass concentrations of $PM_{2.5}$ from 2017 to 2020 were finally chosen for this research. Hourly $PM_{2.5}$ concentrations were similarly categorized into clean conditions ($<$75 μg/m3) and polluted conditions ($>$75 μg/m3) at the time of precipitation events to examine the impact on the accuracy of hourly IMERG precipitation estimates.

Considering that precipitation has a wet scavenging effect on $PM_{2.5}$, we divided the hourly precipitation events under polluted conditions into two types. The precipitation event had a wet scavenging effect on $PM_{2.5}$ when hourly $PM_{2.5}$ concentration was polluted ($>$75 $\mu g/m^3$) 1 h before a precipitation event and was clean ($<$75 $\mu g/m^3$) 1 h after a precipitation event, marked as PC. For well represent the scavenging effect in a PC situation, we removed events where the difference in $PM_{2.5}$ values before and after rainfall was less than 30. The precipitation event had no effect on the removal of $PM_{2.5}$, as evidenced by the fact that the hourly concentration of $PM_{2.5}$ was polluted ($>$75 $\mu g/m^3$) in the hour before the precipitation event, and the hourly concentration of $PM_{2.5}$ was also polluted ($>$75 $\mu g/m^3$) in the hour after the precipitation event, which is expressed as PP. indicated as PP. We marked precipitation events under clean condition as CC.

III. Method

A. Data Matching

A point-to-pixel approach was used to validate the accuracy of the daily and hourly IMERG against rain gauge observations. For consistency with the air monitoring data provided in Beijing Time, the Universal Time Coordinated time of IMERG estimates and the gauge observation data were transformed to local time.

Nearest neighborhood analysis was utilized to match the air monitoring station and the rain gauges. This method measures the distance between each air monitoring station centroid and its nearest rain gauge centroid and finds the nearest neighbor within a 10 km radius. A total of 175 meteorological stations with the nearest air monitoring data were matched in NC as shown in Fig. 3.

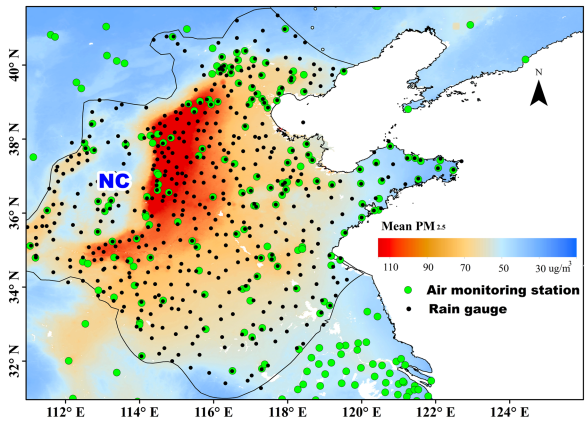

Fig. 3. Spatial distribution of ground air monitoring stations and rain gauges in NC, overlaid on the background of annual average $PM_{2.5}$ concentration distribution from 2014 to 2020.

B. Evaluation Metrics

The performance of IMERG under different atmospheric aerosol concentrations was evaluated by comparing them against ground-based observations with commonly used statics indicators. Normalized root mean squared error (NRMSE) [38], [39] was used to evaluate the precision of IMERG under different atmospheric aerosol concentrations. The probability of detection (POD) and false alarm ratio (FAR) were selected to understand the precipitation capture ability of IMERG. FAR represents the ratio of precipitation identified by satellite when the gauge record shows no rain. The performance metrics were quantified under the different levels of pollution to understand the impact of atmospheric aerosols on the performance of IMERG.

The error decomposition technique can track the error sources and then improve the retrieval algorithms [40], [41]. According to the error decomposition method, the total bias is decomposed into three bias parts, which will provide a more detailed characterization of the IMERG under atmospheric aerosol pollution [2], [40].

$$\text{Total bias} = Hit\ bias - Miss\ bias + False\ bias \quad (1)$$

where $Hit\ bias$ denotes the bias when detection and observation both indicate precipitation. $Miss\ bias$ refers to the bias when detection shows no precipitation but observation shows precipitation. $False\ bias$ is the bias occurring when detection shows precipitation but observation shows no precipitation.

Table I shows the details for the calculation of the above-mentioned metrics.

IV. Results

A. Impact of Atmospheric Aerosols on the Detection Skill of IMERG

To investigate the effect of aerosol pollution on IMERG detection, this study compared the values of POD and FAR under different $PM_{2.5}$ concentrations.

TABLE I
LIST OF FORMULAS USED IN THIS STUDY

Statistical metrics	Equation	The optimal value
Probability of detection	$\mathrm{POD} = \frac{H}{H+M}$	1
False alarm ratio	$\mathrm{FAR} = \frac{F}{H+F}$	0
Normalized root mean square error	$\mathrm{NRMSE} = \sqrt{\frac{1}{N}\sum_{i=1}^{N}(S_i - G_i)^2}/\bar{G}$	0
Bias	$\mathrm{Bias} = \frac{\sum(S-G)}{\sum G} \times 100\%$	0
Hit bias	$\text{Hit bias} = \frac{\sum(S_H - G_H)}{\sum G} \times 100\%$	0
Miss bias	$\text{Miss bias} = \frac{\sum(S_M - G_M)}{\sum G} \times 100\%$	0
False bias	$\text{False bias} = \frac{\sum(S_F - G_F)}{\sum G} \times 100\%$	0

S and G are the estimates from GPM IMERG and observations from gauges. H represents the amount of precipitation events estimated by the GPM IMERG and gauge simultaneously; M represents the amount of rain events measured by the gauge but not recorded by the GPM IMERG. F is the number of false events identified by the GPM IMERG but not observed by the gauge.

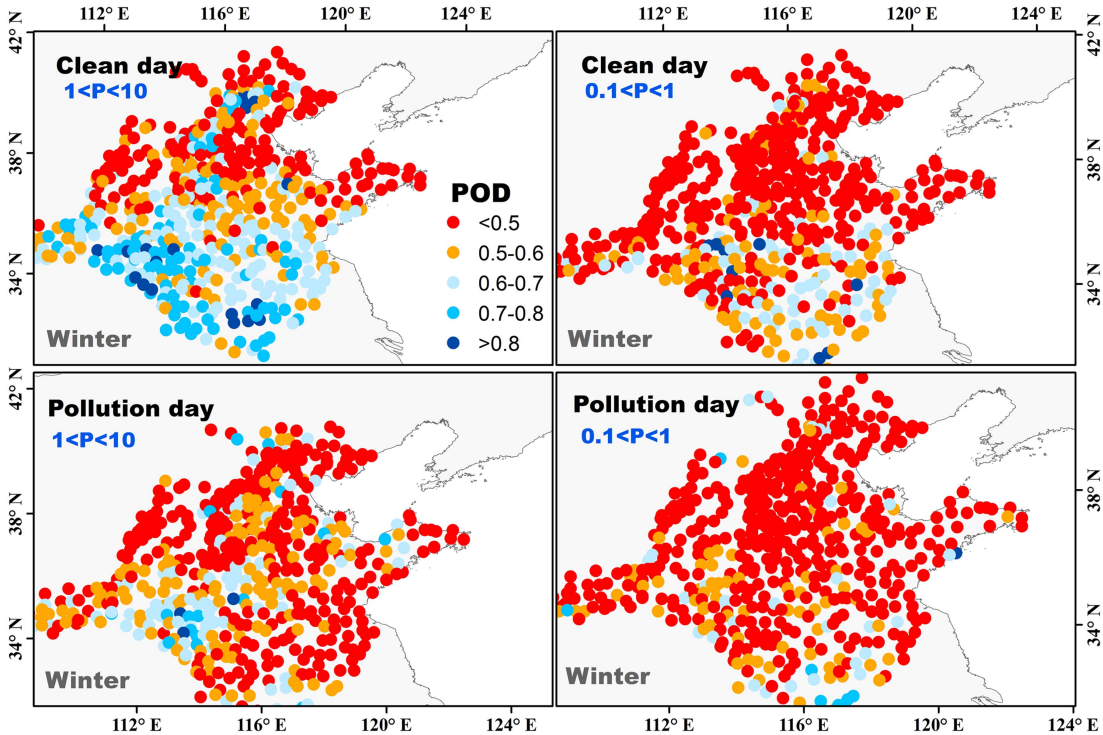

Fig. 4. Spatial distributions of POD under different $PM_{2.5}$ conditions for two rainfall intensity groups.

For IMERG daily products, the spatial distribution of POD under different air conditions for two groups of precipitation intensities in winter is shown in Fig. 4. For drizzle events, IMERG has low POD values in both polluted and clean days. However, for light precipitation, the spatial distribution of POD is markedly variable under polluted and clean days. On clean days, IMERG can detect light precipitation in most areas of NC, with its POD values exceeding 0.7. On polluted days, the POD values drop significantly to less than 0.6 over most of the region.

Fig. 5 also shows that POD above 0.7 in winter are basically distributed on clean days, while the lowest values are distributed on polluted days, further demonstrating the significant decrease

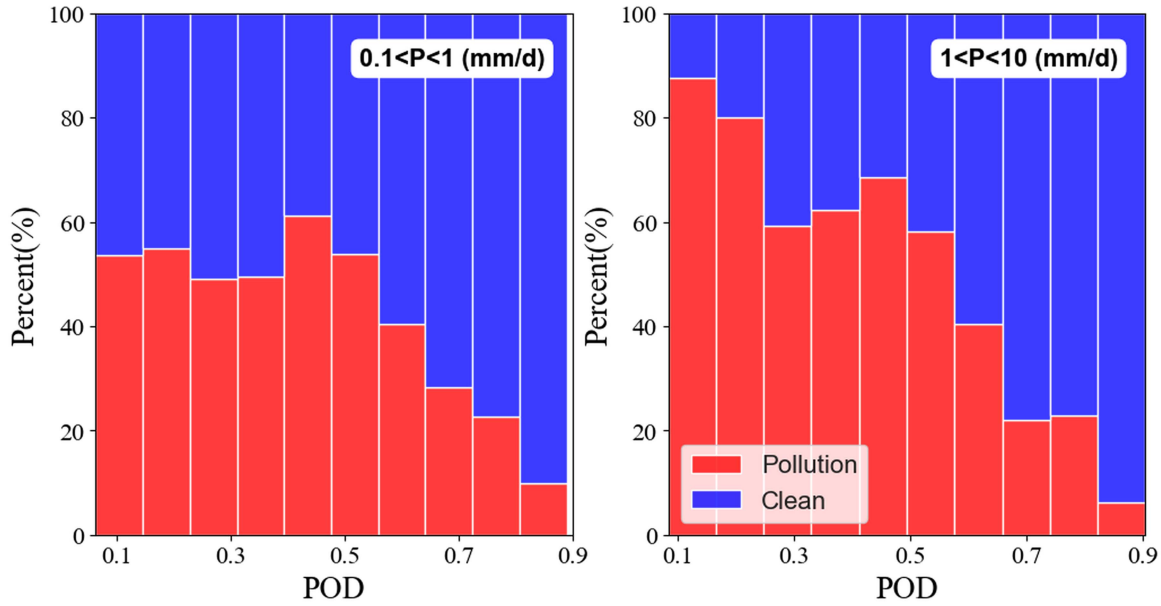

Fig. 5. Histogram of POD under polluted (red) and clean (blue) conditions for two rainfall intensity categories in winter.

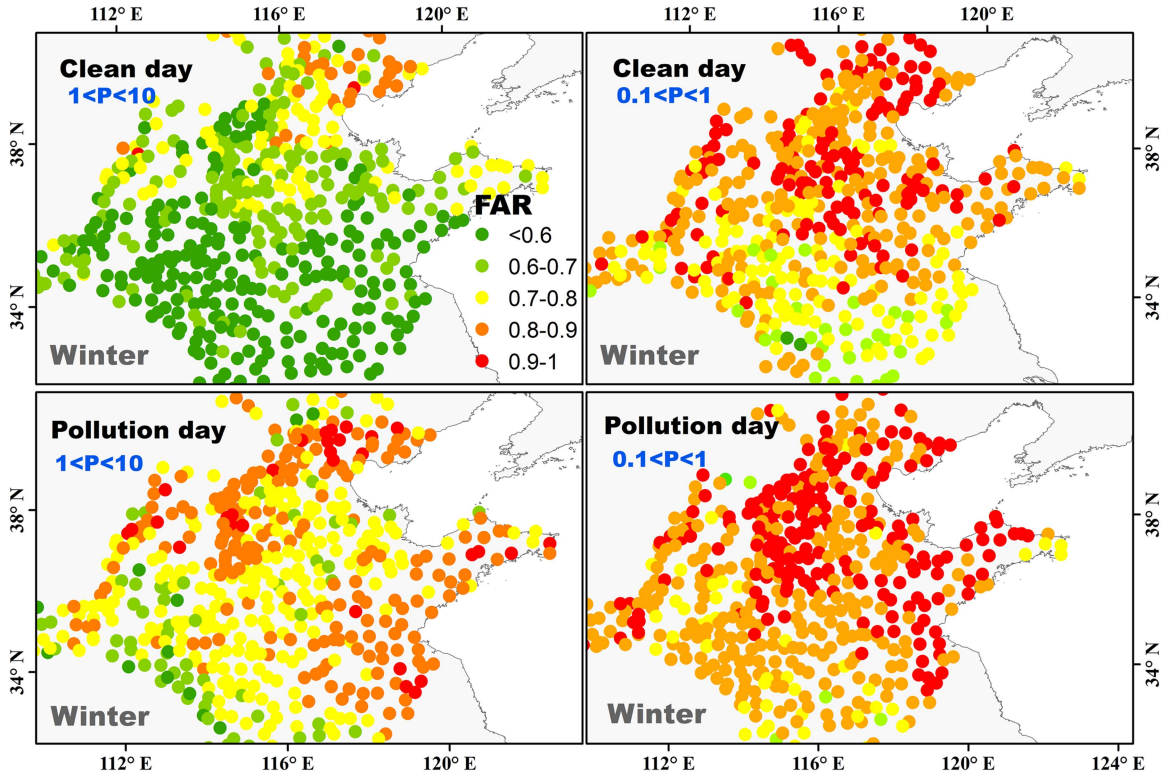

Fig. 6. Spatial distributions of FAR under different $PM_{2.5}$ conditions for two rainfall intensity groups.

in POD values for light precipitation under polluted days. That suggests that the capability of daily IMERG to capture "true" precipitation events (POD) deteriorates in the presence of $PM_{2.5}$ pollution.

For drizzle precipitation, the FAR values of daily IMERG did not show significant differences on clean and polluted days (Fig. 6). However, for light precipitation, the spatial patterns of FAR showed remarkable variation under the two conditions. On clean days, more than 80% of the area had a low FAR value for light precipitation. On polluted days, the FAR values increased significantly in most regions [Fig. 5(b)]. In general, the FAR of IMERG is significantly affected by $PM_{2.5}$ pollution. Fig. 7 shows the histogram of FAR for the two rainfall intensity groups. The distribution of FAR values for light

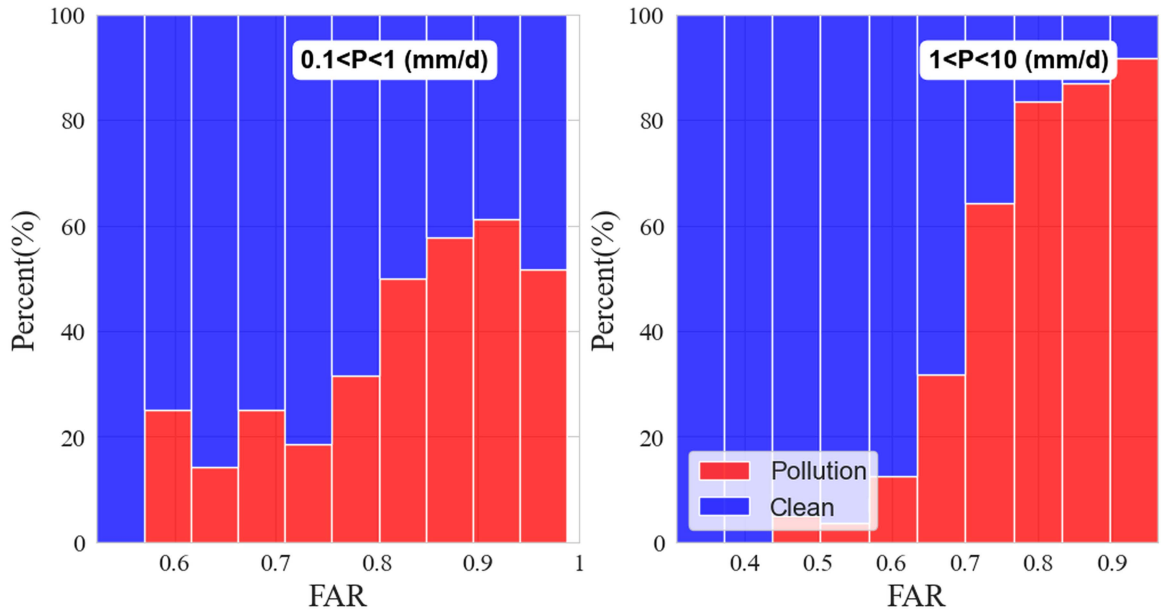

Fig. 7. FAR histogram of daily IMERG under polluted (red) and clean (blue) conditions for two rainfall intensity categories.

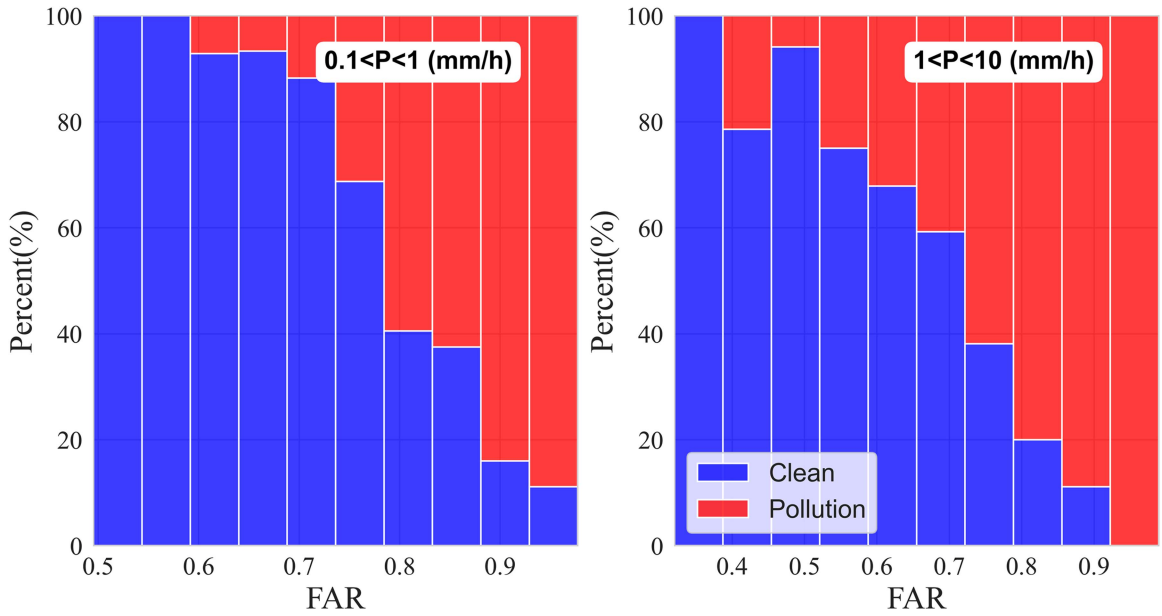

Fig. 8. FAR histogram of hourly IMERG under polluted (red) and clean (blue) conditions for two rainfall intensity categories.

precipitation also shows that polluted days have higher FAR values.

The FAR histogram for hourly IMERG data also shows that the frequency of FAR greater than 0.8 is significantly higher under polluted conditions than in clean conditions (Fig. 8). Based on the above-mentioned analysis, we have found that the FAR of IMERG daily and hourly precipitation data is significantly increased under aerosol polluted conditions. The ratio of events detected by satellite when the gauge record shows that no rain is significantly affected by aerosol pollution.

B. Accuracy Analysis of IMERG Under Two Atmospheric Aerosols Conditions

The boxplot results of bias at the daily scale are presented in Fig. 9. We compared the three components of bias under both clean and polluted days. For miss bias and hit bias, the difference is not obvious in both cases. However, it can be seen that the false bias in the pollution case is much higher than in the clean case. Serious false rainfall estimations of the IMERG mainly occur under polluted conditions. This phenomenon is significant in both winter and autumn.

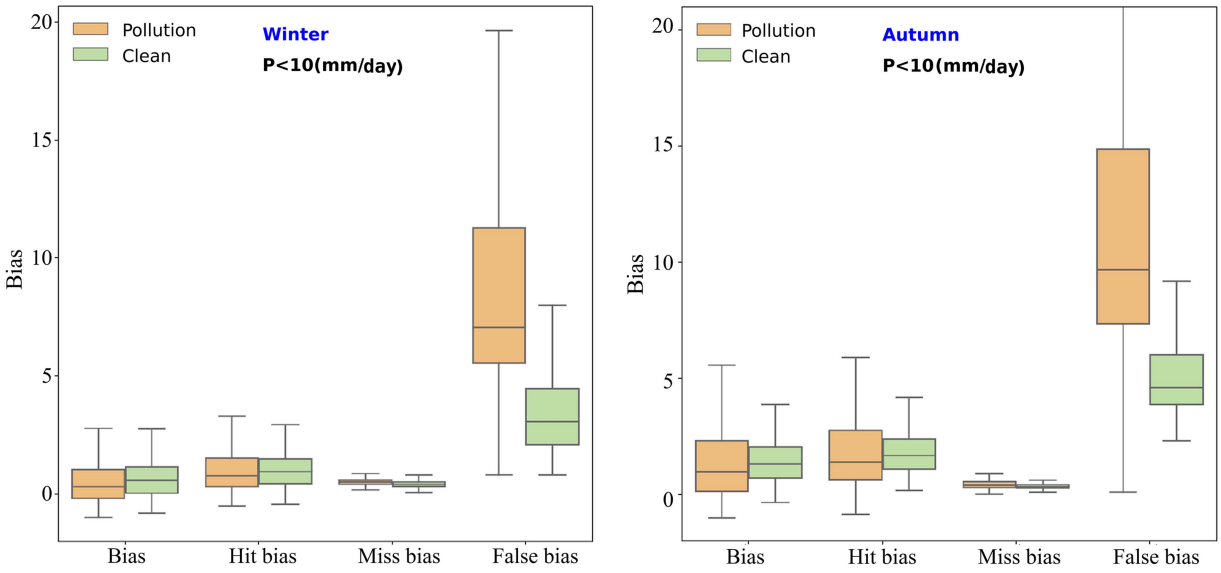

Fig. 9. Boxplots of the relative bias of daily IMERG for two seasons over NC.

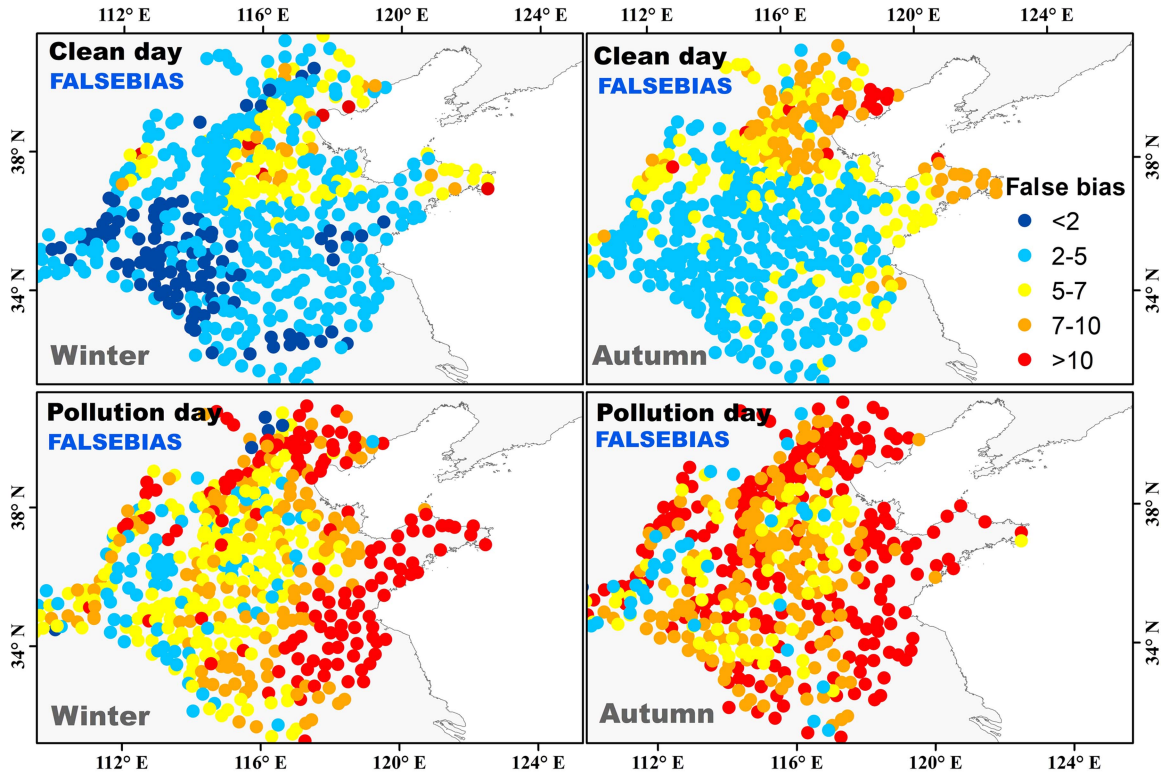

Fig. 10. Spatial distribution of the false bias of daily IMERG for autumn and winter.

The spatial distribution of the false bias score of daily IMERG for the two seasons is shown in Fig. 10. The spatial patterns of false bias greatly differ between clean and polluted days. On clean days, the false bias is smaller in most areas of NC, but higher false bias values are found on polluted days both in winter and autumn. In general, spatial patterns of false bias are consistent with the boxplot analysis result, showing that false bias is closely related to the $PM_{2.5}$ concentrations condition.

Fig. 11 shows a box plot of the bias for the hourly IMERG. The false bias in the hourly scale still shows a clear difference compared to the other bias components. The values of false bias are much larger in the polluted condition than in the clean case.

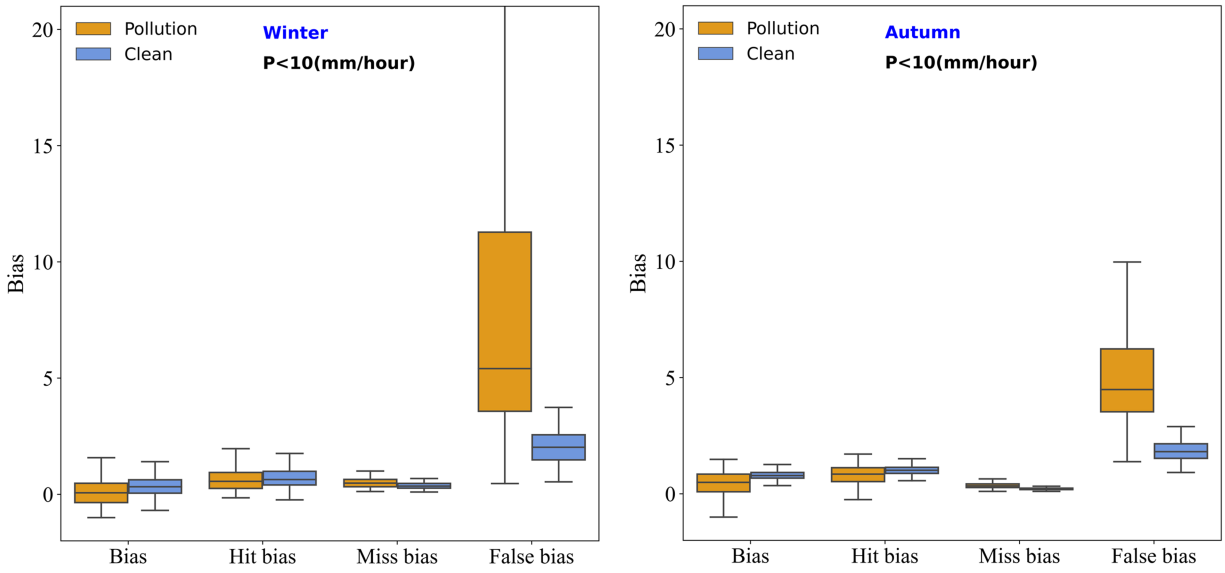

Fig. 11. Boxplots of the relative bias of hourly IMERG for two autumn and winter over NC.

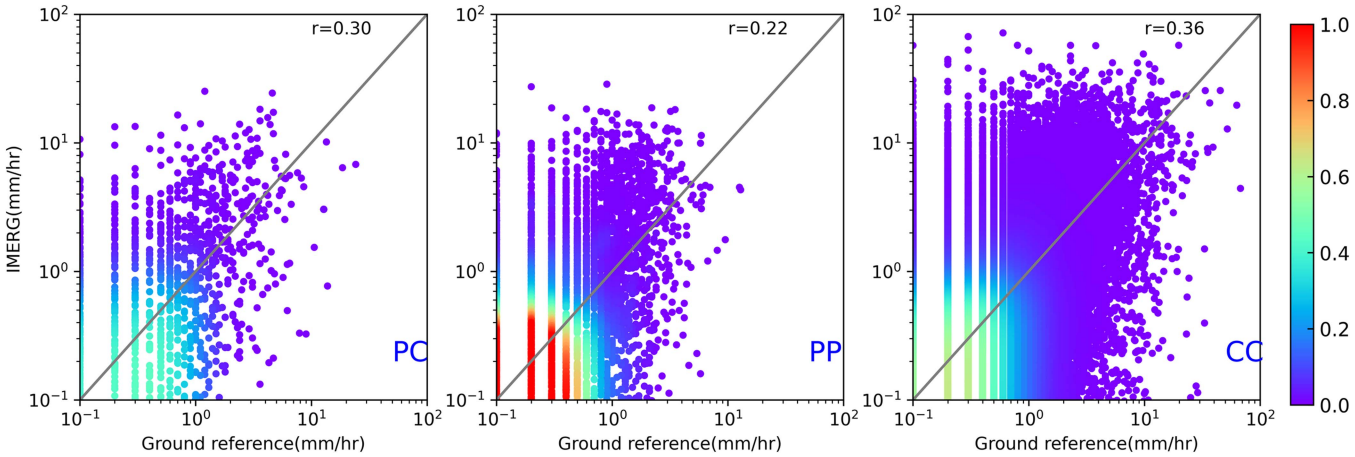

Fig. 12. Density plots of gauge precipitation and IMERG under scavenging situations at the hourly scale. In PP situation, the precipitation event had a wet scavenging effect on $PM_{2.5}$. In PC situations, the precipitation event had no effect on $PM_{2.5}$ removal. In CC situations, the $PM_{2.5}$ is clean before and after the precipitation event.

To achieve a better comprehension of how atmospheric aerosols affect the accuracy of IMERG precipitation estimates, we used the NRMSE to represent the average degree of error under two $PM_{2.5}$ concentration groups. The NRMSE was not significantly different between polluted and clean states on either the daily or the hourly time scale.

C. IMERG Precision Under Different Scavenging Situations

To provide additional insights on the impact of atmospheric aerosols on the precision of hourly IMERG, we divided precipitation under pollution into two categories based on the wet scavenging situation on $PM_{2.5}$. Fig. 12 shows scatter plots of the IMERG versus gauge precipitation under scavenging situations. According to this figure, IMERG under a clean situation (CC) outperforms the products under PC and PP conditions. Scatter points of the IMERG under PC and PP are not only distant from the bisector, but also more dispersed.

The boxplots of the NRMSE for two wet scavenging situations are shown in Fig. 13 . The higher the NRMSE value, the worse the simulation effect of IMERG. NRMSE increased significantly under PP situations for the three rainfall intensity groups. When aerosol pollution is present both before and after a precipitation event it can seriously affect IMERG's precipitation estimate. This may be due to the fact that aerosols can complicate the precipitation process and have an impact on the amount, area, and intensity of precipitation [42], which in turn affects the accuracy of IMERG.

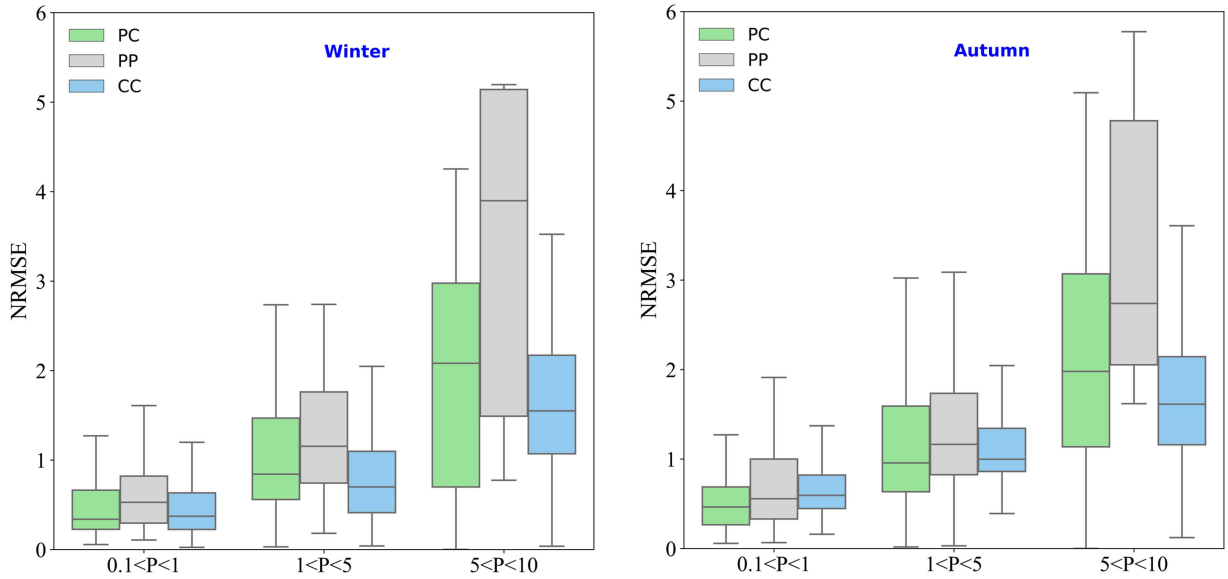

Fig. 13. Boxplots of NRMSE for two wet scavenging situations.

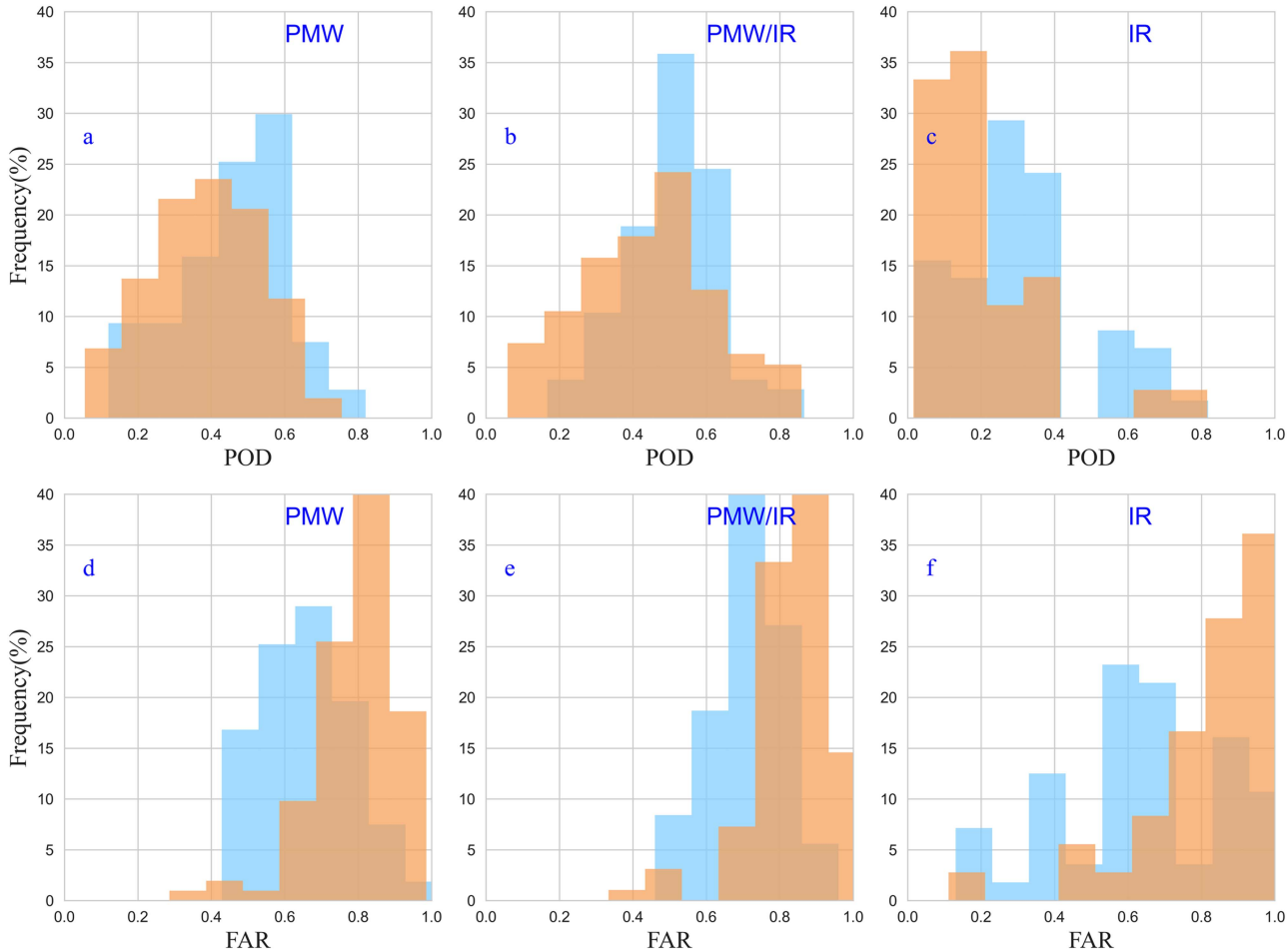

Fig. 14. POD (first row), FAR (second row) PDFs of different sensors. Orange and blue correspond to observations under polluted and clean conditions in winter.

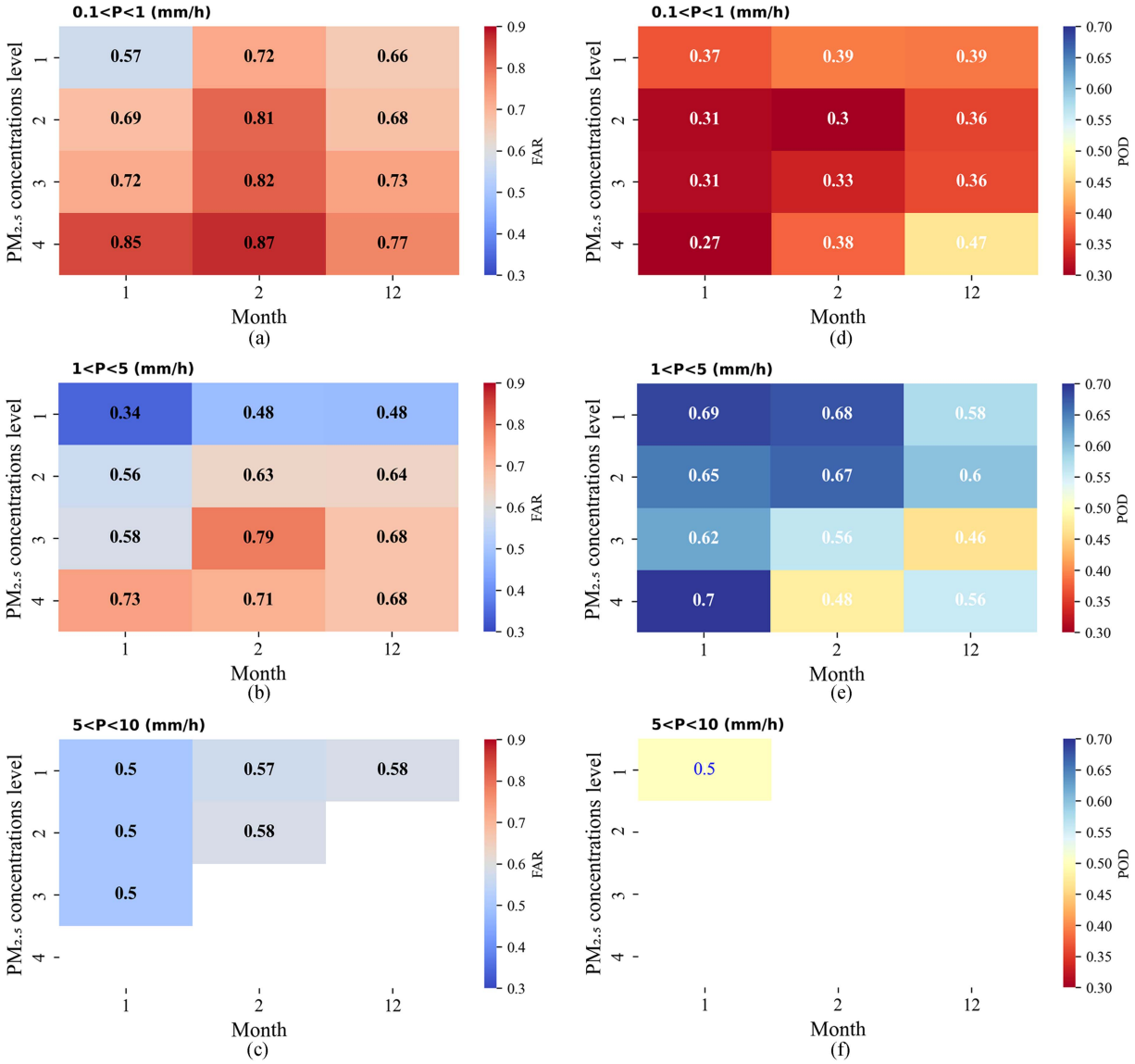

Fig. 15. Heatmap of precipitation detection scores of each precipitation class under four pollution levels. (a) FAR of IMERG for rain rates less than 1 mm/h, (b) FAR of IMERG for rain rates between 1 and 5 mm/h, (c) FAR of IMERG for rain rates between 5 and 10 mm/h, (d) POD of IMERG for rain rates less than 1 mm/h, (e) POD of IMERG for rain rates between 1 and 5 mm/h, (f) POD of IMERG for rain rates between 5 and 10 mm/h.

D. How Do Atmospheric Aerosols Impact the Detection Performance of Different Sensors

To improve the detectability of IMERG under polluted conditions, it is necessary to understand the uncertainties of the sensors. Fig. 14 illustrates the detection performance of PMW, IR, and combined PMW/IR data under polluted and clean conditions in winter by using POD [Fig. 14(a)–(c)] and FAR [Fig. 14(d)–(f)].

Fig. 14 showed that PMW data have similar POD values under polluted and clean conditions. However, IR under polluted conditions has a lower POD distribution than under clean conditions. Both PMW and IR estimates display higher FAR under polluted than in clean conditions, meaning that each sensor detected significant precipitation events in polluted conditions when the gauge record showed no rain. The detection capability of IR and PMW estimates is significantly affected by atmospheric aerosols.

This may be related to the different impacts of aerosol pollution on PMW and IR precipitation estimates. PMW can probe through most of the clouds and directly estimate the precipitation from the scattering properties of a vertical column of cloud and hydrometeors [43], [44]. On the other hand, using IR imagery to estimate precipitation is typically relied upon the brightness temperature of the cloud top, which is correlated with the surface precipitation rate [45]. Aerosols affect reflectance and cloud brightness [46], [47]. Cloud top temperatures are significantly correlated with increasing aerosol concentrations [48]. By influencing cloud top temperatures, aerosols may affect precipitation estimates of IR.

V. Discussion

Our results analysis revealed that pollution exerts a significant influence on the detection scores of IMERG. This raises the question of whether the FAR and POD escalate with increasing

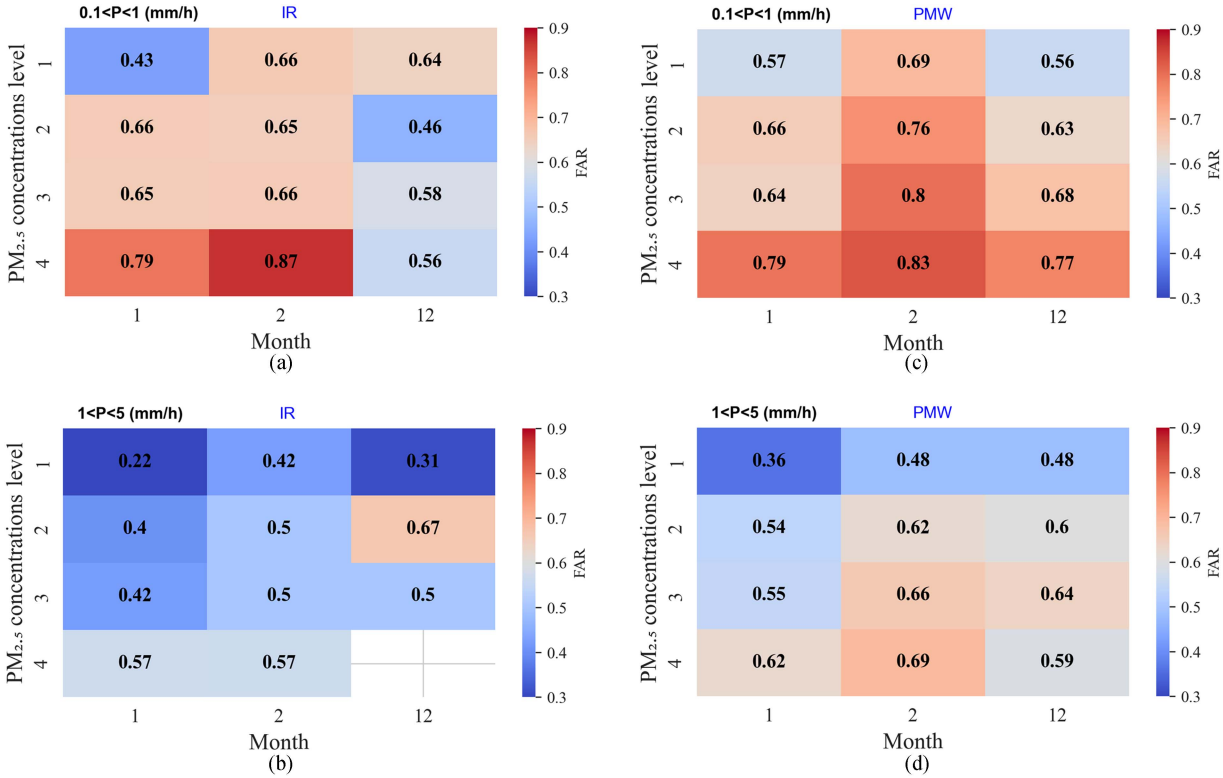

Fig. 16. Heatmap of FAR under four pollution levels of different sensors in winter. (a) FAR of IR for rain rates less than 1 mm/h, (b) FAR of IR for rain rates between 1 and 5 mm/h, (c) FAR of PMW for rain rates less than 1 mm/h, (d) FAR of PMW for rain rates between 1 and 5 mm/h.

pollutant concentration. To address this inquiry, we performed additional analysis. Hourly precipitation and $PM_{2.5}$ data from the winter season were used to examine the changes in the detection scores across varying pollution concentrations. The precipitation was categorized into three classes: less than 1 mm/h, 1 to 5 mm/h, and 5 to 10 mm/h. We categorized the pollutant concentrations into four levels: 0–35 as level 1, 35–75 as level 2, 75–105 as level 3, and greater than 105 as level 4. The FAR and POD of each precipitation class under different pollution levels were then calculated.

As illustrated in Fig. 15(a), FAR for rain rates less than 1 mm/h exhibited an increasing trend with escalating pollution levels in all months. This indicates that escalating pollution causes satellite-based precipitation detection to identify considerably more rainfall events that are not confirmed by ground-based gauge measurements. For rain rates between 1 and 5 mm/h [Fig. 15(b)], the FAR continued to demonstrate an upward trend with rising pollution levels. However, for rain rates between 5 and 10 mm/h [Fig. 15(c)], intensifying pollution levels did not exert discernible influence on the FAR.

As depicted in Fig. 15(d)–(f), in some scenarios, such as rain events of 0.1–1 mm/h in January and rain events of 1–5 mm/h in February, there exhibited a declining trend in POD with intensifying pollution. However, overall across all rain types and months, there was no such discernible trend.

We further conducted the analysis from the perspective of sensors. As shown in Fig. 16, for precipitation below 5 mm/h, with intensifying pollution, FAR of both PMW and IR sensors exhibited a stepwise increasing trend. PMW and IR sensors. For PMW sensors, pollutants absorb microwaves and attenuate microwave signals, which can lead to erroneous detection of precipitation signals. As for IR sensors, high aerosol concentrations result in increased radiance temperatures at the top of the atmosphere [45]. IR sensors infer the presence of clouds and precipitation based on changes in radiance temperatures [49]. Thus, the heightened radiance temperatures caused by pollutants can be incorrectly interpreted as the existence of clouds or precipitation.

The heat map distribution in Fig. 17 demonstrates distinct variations in the POD for IR and PMW sensors as pollution levels intensify. The POD for IR sensors decreases as pollution increases. In contrast, the POD for PMW sensors is insensitive to changes in pollution concentrations. PMW sensors detect precipitation by measuring the attenuation of microwave signals. While pollutants can absorb microwaves and lead to signal attenuation, this attenuation is seldom greater than that caused by rainfall. Thus, PMW sensors can still detect precipitation if rain droplets induce sufficient microwave attenuation, even under polluted conditions. In contrast, IR sensors infer clouds and precipitation based on the radiance temperature at the top of the atmosphere. When concentrations of pollutants (especially aerosols) increase, more IR radiation is absorbed and scattered, leading to elevated detected radiance temperatures. Under heavy pollution, particularly for light rainfall below 1 mm/h, IR sensors struggle to discriminate whether heightened radiance temperatures are due to pollution or actual clouds/rainfall.

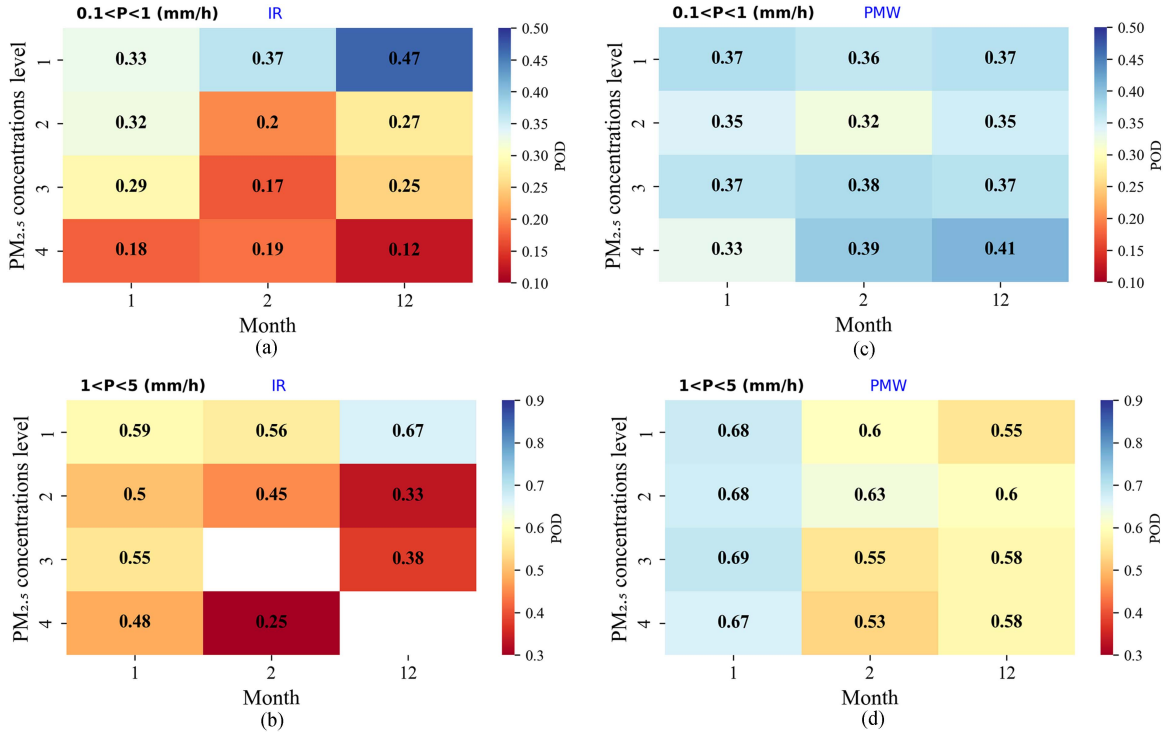

Fig. 17. Heatmap of POD under four pollution levels of different sensors in winter. (a) POD of IR for rain rates less than 1 mm/h, (b) POD of IR for rain rates between 1 and 5 mm/h, (c) POD of PMW for rain rates less than 1 mm/h, (b) POD of PMW for rain rates between 1 and 5 mm/h.

Under the four levels of pollution, the changes in POD values of PWM and IR sensors are markedly different, which further explains the statistical trends of POD values in Fig. 14. When we analyze the POD changes of IMERG products under pollution, the change trend of pixels that are a mixture of PMW and IR will be unclear.

VI. Conclusion

The influence of atmospheric aerosols on the reliability of IMERG precipitation estimates was explored over NC in this article. We compared IMERG with a gauge dataset under polluted and clean conditions.

Based on a comprehensive analysis, the primary findings are summarized as follows.

1) The influence of atmospheric aerosols on the detectability of IMERG is significant. IMERG generally exhibits better detectability (higher POD and lower FAR) and quantification (lower NRMSE) under clean conditions. IMERG tends to detect more precipitation events in the presence of pollution when the gauge record shows no rain. Specifically, in autumn and winter when aerosol pollution primarily arises, the false bias constitutes the predominant proportion of the total bias.
2) From the sensor perspective, for light rainfall events less than 5 mm/h, as the degree of pollution intensifies, FAR of both PMW radiometers and IR sensors shows an increasing trend. Meanwhile, the POD of IR sensors decreases as the pollution intensifies, but the POD value of PMW radiometers does not change.
3) Compared to precipitation events with a wet scavenging effect, IMERG has higher NRMSE values when precipitation does not remove $PM_{2.5}$ pollution. That is to say, the precision of IMERG under atmospheric aerosol pollution has a deviation.

This study aims to enhance our fundamental understanding of the accuracy of IMERG precipitation estimates under aerosol pollution. The analysis of satellite precipitation data quality under atmospheric aerosols leads to an improved awareness of the evaluation uncertainty of IMERG precipitation products and contributes to subsequent algorithm improvements.

Acknowledgment

The authors would like to thank the GPM science team for providing access to the IMERG products, the CMA for supplying the MPA data, and all the anonymous reviewers and editors for their helpful comments and suggestions. The computation for this work is supported by the Supercomputing Centre of Lanzhou University.

References

[1] C. Kidd and G. Huffman, "Global precipitation measurement," *Meteorol. Appl.*, vol. 18, no. 3, pp. 334–353, Sep. 2011, doi: 10.1002/met.284.
[2] H. Q. Chen, B. Yong, P. E. Kirstetter, L. Y. Wang, and Y. Hong, "Global component analysis of errors in three satellite-only global precipitation estimates," *Hydrol. Earth Syst. Sci.*, vol. 25, no. 6, pp. 3087–3104, Jun. 2021, doi: 10.5194/hess-25-3087-2021.
[3] G. Q. Tang, M. P. Clark, S. M. Papalexiou, Z. Q. Ma, and Y. Hong, "Have satellite precipitation products improved over last two decades? A comprehensive comparison of GPM IMERG with nine satellite and reanalysis

datasets," *Remote Sens. Environ.*, vol. 240, Apr. 2020, Art. no. 111697, doi: 10.1016/j.rse.2020.111697.

[4] R. K. Pradhan et al., "Review of GPM IMERG performance: A global perspective," *Remote Sens. Environ.*, vol. 268, Jan. 2022, Art. no. 112754, doi: 10.1016/j.rse.2021.112754.

[5] Z. Q. Ma, Z. Shi, Y. Zhou, J. F. Xu, W. Yu, and Y. Y. Yang, "A spatial data mining algorithm for downscaling TMPA 3B43 V7 data over the Qinghai–Tibet Plateau with the effects of systematic anomalies removed," *Remote Sens. Environ.*, vol. 200, pp. 378–395, Oct. 2017, doi: 10.1016/j.rse.2017.08.023.

[6] J. Tan, G. J. Huffman, D. T. Bolvin, and E. J. Nelkin, "IMERG V06: Changes to the morphing algorithm," *J. Atmospheric Ocean. Technol.*, vol. 36, no. 12, pp. 2471–2482, Dec. 2019, doi: 10.1175/Jtech-D-19-0114.1.

[7] G. Skofronick-Jackson, G. Huffman, and W. Petersen, "Three years of the global precipitation measurement (GPM) mission," in *Proc. IEEE Int. Geosci. Remote Sens. Symp.*, 2017, pp. 2704–2707.

[8] A. S. Gebregiorgis et al., "To what extent is the day 1 GPM IMERG satellite precipitation estimate improved as compared to TRMM TMPA-RT?," *J. Geophysical Res.: Atmospheres*, vol. 123, no. 3, pp. 1694–1707, Feb. 2018, doi: 10.1002/2017jd027606.

[9] J. Tan, G. J. Huffman, D. T. Bolvin, and E. J. Nelkin, "Diurnal cycle of IMERG V06 precipitation," *Geophysical Res. Lett.*, vol. 46, no. 22, pp. 13584–13592, Nov. 2019, doi: 10.1029/2019gl085395.

[10] M. N. Anjum et al., "Performance evaluation of latest integrated multi-satellite retrievals for global precipitation measurement (IMERG) over the northern highlands of Pakistan," *Atmospheric Res.*, vol. 205, pp. 134–146, Jun. 2018, doi: 10.1016/j.atmosres.2018.02.010.

[11] O. Sungmin and P.-E. Kirstetter, "Evaluation of diurnal variation of GPM IMERG-derived summer precipitation over the contiguous US using MRMS data," *Quart. J. Roy. Meteorological Soc.*, vol. 144, no. S1, pp. 270–281, 2018, doi: 10.1002/qj.3218.

[12] G. Q. Tang et al., "Statistical and hydrological comparisons between TRMM and GPM level-3 products over a midlatitude basin: Is day-1 IMERG a good successor for TMPA 3B42V7?," *J. Hydrometeorology*, vol. 17, no. 1, pp. 121–137, Jan. 2016, doi: 10.1175/Jhm-D-15-0059.1.

[13] M. F. R. Gaona, A. Overeem, A. M. Brasjen, J. F. Meirink, H. Leijnse, and R. Uijlenhoet, "Evaluation of rainfall products derived from satellites and microwave links for The Netherlands," *IEEE Trans. Geosci. Remote Sens.*, vol. 55, no. 12, pp. 6849–6859, Dec. 2017, doi: 10.1109/Tgrs.2017.2735439.

[14] N. Li, G. Q. Tang, P. Zhao, Y. Hong, Y. B. Gou, and K. Yang, "Statistical assessment and hydrological utility of the latest multi-satellite precipitation analysis IMERG in Ganjiang River basin," *Atmospheric Res.*, vol. 183, pp. 212–223, Jan. 2017, doi: 10.1016/j.atmosres.2016.07.020.

[15] R. Zubieta, A. Getirana, J. C. Espinoza, W. Lavado-Casimiro, and L. Aragon, "Hydrological modeling of the Peruvian–Ecuadorian Amazon Basin using GPM-IMERG satellite-based precipitation dataset," *Hydrol. Earth Syst. Sci.*, vol. 21, no. 7, pp. 3543–3555, Jul. 2017, doi: 10.5194/hess-21-3543-2017.

[16] J. B. Su, H. S. Lu, W. T. Crow, Y. H. Zhu, and Y. F. Cui, "The effect of spatiotemporal resolution degradation on the accuracy of IMERG products over the Huai River basin," *J. Hydrometeorology*, vol. 21, no. 5, pp. 1073–1088, May 2020, doi: 10.1175/Jhm-D-19-0158.1.

[17] J. Tan, W. A. Petersen, and A. Tokay, "A novel approach to identify sources of errors in IMERG for GPM ground validation," *J. Hydrometeorology*, vol. 17, no. 9, pp. 2477–2491, Sep. 2016, doi: 10.1175/Jhm-D-16-0079.1.

[18] C. Chen et al., "Triple collocation-based error estimation and data fusion of global gridded precipitation products over the Yangtze River basin," *J. Hydrometeorology*, vol. 605, Feb. 2022, Art. no. 127307, doi: 10.1016/j.jhydrol.2021.127307.

[19] S. Y. Zhu, Y. Shen, and Z. Q. Ma, "A new perspective for characterizing the spatio-temporal patterns of the error in GPM IMERG over mainland China," *Earth Space Sci.*, vol. 8, no. 1, Jan. 2021, p. 1, doi: 10.1029/2020EA001232.

[20] X. Li, O. Sungmin, N. Wang, L. Liu, and Y. Huang, "Evaluation of the GPM IMERG V06 products for light rain over Mainland China," *Atmospheric Res.*, vol. 253, May 2021, Art. no. 105510, doi: 10.1016/j.atmosres.2021.105510.

[21] M. Kumar, O. Hodnebrog, A. S. Daloz, S. Sen, S. Badiger, and J. Krishnaswamy, "Measuring precipitation in Eastern Himalaya: Ground validation of eleven satellite, model and gauge interpolated gridded products," *J. Hydrol.*, vol. 599, Aug. 2021, Art. no. 126252, doi: 10.1016/j.jhydrol.2021.126252.

[22] D. Rosenfeld et al., "Flood or drought: How do aerosols affect precipitation?," *Science*, vol. 321, no. 5894, pp. 1309–1313, Sep. 2008, doi: 10.1126/science.1160606.

[23] B. Stevens and G. Feingold, "Untangling aerosol effects on clouds and precipitation in a buffered system," *Nature*, vol. 461, no. 7264, pp. 607–613, Oct. 2009, doi: 10.1038/nature08281.

[24] Z. S. Xiao, S. B. Zhu, Y. C. Miao, Y. Yu, and H. Z. Che, "On the relationship between convective precipitation and aerosol pollution in North China Plain during autumn and winter," *Atmospheric Res.*, vol. 271, Jun. 2022, Art. no. 106120, doi: 10.1016/j.atmosres.2022.106120.

[25] J. F. Peng et al., "Explosive secondary aerosol formation during severe haze in the North China Plain," *Environ. Sci. Technol.*, vol. 55, no. 4, pp. 2189–2207, Feb. 2021, doi: 10.1021/acs.est.0c07204.

[26] Q. Zhu, L. M. Cao, M. X. Tang, X. F. Huang, E. Saikawa, and L. Y. He, "Characterization of organic aerosol at a rural site in the North China Plain region: Sources, volatility and organonitrates," *Adv. Atmospheric Sci.*, vol. 38, no. 7, pp. 1115–1127, Jul. 2021, doi: 10.1007/s00376-020-0127-2.

[27] H. Y. Li et al., "Wintertime aerosol chemistry and haze evolution in an extremely polluted city of the North China Plain: Significant contribution from coal and biomass combustion," *Atmospheric Chem. Phys.*, vol. 17, no. 7, pp. 4751–4768, Apr. 2017, doi: 10.5194/acp-17-4751-2017.

[28] W. Q. Xu et al., "Organic aerosol volatility and viscosity in the North China Plain: Contrast between summer and winter," *Atmospheric Chem. Phys.*, vol. 21, no. 7, pp. 5463–5476, Apr. 2021, doi: 10.5194/acp-21-5463-2021.

[29] J. Li et al., "Winter particulate pollution severity in North China driven by atmospheric teleconnections," *Nature Geosci.*, vol. 15, no. 5, pp. 349–355, May 2022, doi: 10.1038/s41561-022-00933-2.

[30] M. Zhang et al., "Haze events at different levels in winters: A comprehensive study of meteorological factors, aerosol characteristics and direct radiative forcing in megacities of north and central China," *Atmospheric Environ.*, vol. 245, Jan. 2021, Art. no. 118056, doi: 10.1016/j.atmosenv.2020.118056.

[31] Q. Li, B. Wu, J. Liu, H. Zhang, X. Cai, and Y. Song, "Characteristics of the atmospheric boundary layer and its relation with $PM_{2.5}$ during haze episodes in winter in the North China Plain," *Atmospheric Environ.*, vol. 223, Feb. 2020, Art. no. 117265, doi: 10.1016/j.atmosenv.2020.117265.

[32] G. J. B. Huffman et al., "NASA global precipitation measurement integrated multisatellite retrievals for GPM (IMERG) algorithm theoretical basis document (ATBD) version 06.," 2019. [Online]. Available: https://gpm.nasa.gov/sites/default/files/document_files/IMERG_ATBD_V06.pdf

[33] G. J. Huffman, *Satellite Precipitation Measurement*, vol. 1, V. Levizzani, C. Kidd, D. B. Kirschbaum, C. D. Kummerow, K. Nakamura, and F. J. Turk, Eds. Berlin, Germany: Springer-Verlag, 2020.

[34] A.-P. Kazamias, M. Sapountzis, and K. Lagouvardos, "Evaluation of GPM-IMERG rainfall estimates at multiple temporal and spatial scales over Greece," *Atmospheric Res.*, vol. 269, May 2022, Art. no. 106014, doi: 10.1016/j.atmosres.2021.106014.

[35] J. Wei and Z. Q. Li, *ChinaHighPM$_{2.5}$: Big Data Seamless 1 km Ground-level PM$_{2.5}$ Dataset for China (2000-2021)*, National Tibetan Plateau/Third Pole Environment Data Center, doi: 10.5281/zenodo.3539349.

[36] J. Wei et al., "Reconstructing 1-km-resolution high-quality $PM_{2.5}$ data records from 2000 to 2018 in China: Spatiotemporal variations and policy implications," *Remote Sens. Environ.*, vol. 252, Jan. 2021, Art. no. 112136, doi: 10.1016/j.rse.2020.112136.

[37] Y. Zhao et al., "Unsupervised $PM_{2.5}$ anomalies in China induced by the COVID-19 epidemic," *Sci. Total Environ.*, vol. 795, Nov. 2021, Art. no. 148807, doi: 10.1016/j.scitotenv.2021.148807.

[38] A. Ghomlaghi, M. Nasseri, and B. Bayat, "Comparing and contrasting the performance of high-resolution precipitation products via error decomposition and triple collocation: An application to different climate classes of the central Iran," *J. Hydrol.*, vol. 612, Sep. 2022, Art. no. 128298, doi: 10.1016/j.jhydrol.2022.128298.

[39] H. Q. Chen, B. Yong, W. Q. Qi, H. Wu, L. L. Ren, and Y. Hong, "Investigating the evaluation uncertainty for satellite precipitation estimates based on two different ground precipitation observation products," *J. Hydrometeorology*, vol. 21, no. 11, pp. 2595–2606, Nov. 2020, doi: 10.1175/Jhm-D-20-0103.1.

[40] Y. D. Tian et al., "Component analysis of errors in satellite-based precipitation estimates," *J. Geophysical Res.: Atmospheres*, vol. 114, no. D24, Dec. 2009, doi: 10.1029/2009jd011949.

[41] G. Tang, M. P. Clark, S. M. Papalexiou, Z. Ma, and Y. Hong, "Have satellite precipitation products improved over last two decades? A comprehensive comparison of GPM IMERG with nine satellite and reanalysis datasets," *Remote Sens. Environ.*, vol. 240, Apr. 2020, Art. no. 111697, doi: 10.1016/j.rse.2020.111697.
[42] Y. Sun and C. Zhao, "Distinct impacts on precipitation by aerosol radiative effect over three different megacity regions of eastern China," *Atmospheric Chem. Phys.*, vol. 21, no. 21, pp. 16555–16574, 2021, doi: 10.5194/acp-21-16555-2021.
[43] C. Kidd and V. Levizzani, "Status of satellite precipitation retrievals," *Hydrol. Earth Syst. Sci.*, vol. 15, no. 4, pp. 1109–1116, 2011, doi: 10.5194/hess-15-1109-2011.
[44] M. Sadeghi, P. Nguyen, K. Hsu, and S. Sorooshian, "Improving near real-time precipitation estimation using a U-Net convolutional neural network and geographical information," *Environ. Model. Softw.*, vol. 134, Dec. 2020, Art. no. 104856, doi: 10.1016/j.envsoft.2020.104856.
[45] M. Ombadi, P. Nguyen, S. Sorooshian, and K.-l. Hsu, "How much information on precipitation is contained in satellite infrared imagery?," *Atmospheric Res.*, vol. 256, Jul. 2021, Art. no. 105578, doi: 10.1016/j.atmosres.2021.105578.
[46] M. W. Christensen, W. K. Jones, and P. Stier, "Aerosols enhance cloud lifetime and brightness along the stratus-to-cumulus transition," *Proc. Nat. Acad. Sci.*, vol. 117, no. 30, pp. 17591–17598, 2020, doi: 10.1073/pnas.1921231117.
[47] Y. Chen et al., "Machine learning reveals climate forcing from aerosols is dominated by increased cloud cover," *Nature Geosci.*, vol. 15, no. 8, pp. 609–614, Aug. 2022, doi: 10.1038/s41561-022-00991-6.
[48] F. Niu and Z. Li, "Systematic variations of cloud top temperature and precipitation rate with aerosols over the global tropics," *Atmospheric Chem. Phys.*, vol. 12, no. 18, pp. 8491–8498, 2012, doi: 10.5194/acp-12-8491-2012.
[49] P. Nguyen et al., "PERSIANN dynamic infrared–rain rate model (PDIR) for high-resolution, real-time satellite precipitation estimation," *Bull. Amer. Meteorological Soc.*, vol. 101, no. 3, pp. E286–E302, Mar. 2020, doi: 10.1175/BAMS-D-19-0118.1.

Xiaoying Li received the B.E. degree in geographic information system and the M.S. degree in human geography from Lanzhou University, Lanzhou, China, in 2004 and 2007, respectively, and the Ph.D. degree in physical geography from the University of Chinese Academy of Sciences, Beijing, China, in 2013.

Her research interests include application of remote sensing in hydrology and urban environmental remote sensing, with a focus on developing high-quality satellite precipitation products for cold alpine region.

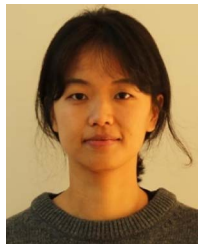

Sungmin O received the Ph.D. degree in physics (meteorology) from the University of Graz, Graz, Austria, in 2018.

She worked as a Postdoctoral Researcher with the Max Planck Institute for Biogeochemistry, Germany, and she is currently a Research Professor with the Department of Climate and Energy System Engineering, Ewha Womans University, Seoul, South Korea. Her research interests include big data processing, hydrologic modeling, machine learning, and land-atmosphere interactions.

Na Wang received the M.S. degree in atmospheric physics and atmospheric environment from Lanzhou University, Lanzhou, China, in 2007.

She is currently working with Shaanxi Climate Center, Xi'an, China. Her research interests include climate and climate change.

Lichen Liu received the B.E. degree in physical geography, the M.S. degree in human geography, and the Ph.D. degree in physical geography from Lanzhou University, Lanzhou, China, in 2003, 2005, and 2008, respectively.

His research interests include water environment protection, environmental planning, and regional sustainable development.

Yinzhou Huang received the B.S. degree in computer science and the Ph.D. degree in human geography from Lanzhou University, Lanzhou, China, in 2004, and 2009, respectively.

He is currently a Professor with the College of Earth and Environmental Sciences, Lanzhou University. His research interests include ecological conservation, regional development, and urban remote-sensing computing.